Dual personality of GABA/glycine-mediated depolarizations in immature spinal cord

Céline Jean-Xavier*, George Z. Mentis†, Michael J. O'Donovan†, Daniel Cattaert‡, and Laurent Vinay*§

*Laboratoire Plasticité et Physio-Pathologie de la Motricité, Centre National de la Recherche Scientifique, Aix-Marseille Université, 31 Chemin Joseph Aiguier, F-13402 Marseille Cedex 20, France; ‡Laboratoire de Neurobiologie des Réseaux, Centre National de la Recherche Scientifique, Université de Bordeaux, 1 Avenue des Facultés, 33405 Talence Cedex, France; and †Laboratory of Neural Control, National Institute of Neurological Disorders and Stroke, National Institutes of Health, Bethesda, MD 20892

Communicated by Lynn T. Landmesser, Case Western Reserve University, Cleveland, OH, May 25, 2007 (received for review October 18, 2006)

The inhibitory action of glycine and GABA in adult neurons consists of both shunting incoming excitations and moving the membrane potential away from the action potential (AP) threshold. By contrast, in immature neurons, inhibitory postsynaptic potentials (IPSPs) are depolarizing; it is generally accepted that, despite their depolarizing action, these IPSPs are inhibitory because of the shunting action of the Cl^- conductance increase. Here we investigated the integration of depolarizing IPSPs (dIPSPs) with excitatory inputs in the neonatal rodent spinal cord by means of both intracellular recordings from lumbar motoneurons and a simulation using the compartment model program "Neuron." We show that the ability of IPSPs to suppress suprathreshold excitatory events depends on E_{Cl} and the location of inhibitory synapses. The depolarization outlasts the conductance changes and spreads electrotonically in the somatodendritic tree, whereas the shunting effect is restricted and local. As a consequence, dIPSPs facilitated AP generation by subthreshold excitatory events in the late phase of the response. The window of facilitation became wider as E_{Cl} was more depolarized and started earlier as inhibitory synapses were moved away from the excitatory input. GAD65/67 immunohistochemistry demonstrated the existence of distal inhibitory synapses on motoneurons in the neonatal rodent spinal cord. This study demonstrates that small dIPSPs can either inhibit or facilitate excitatory inputs depending on timing and location. Our results raise the possibility that inhibitory synapses exert a facilitatory action on distant excitatory inputs and slight changes of E_{Cl} may have important consequences for network processing.

chloride homeostasis | facilitation | inhibition | synaptic integration

GABA and glycine are excitatory in the immature spinal cord and become inhibitory during development. The shift from depolarizing to hyperpolarizing inhibitory postsynaptic potentials (IPSPs) occurs during the first postnatal week (1), a time window during which motoneurons (MNs) undergo considerable maturation of membrane properties (see ref. 2 for review). Some 15 years after the demonstration that GABA and glycine depolarize immature neurons (3–12), the excitatory or inhibitory nature of these depolarizations is still a matter of debate. A critical factor appears to be the equilibrium potential for Cl^- ions (E_{Cl}) relative to action potential (AP) threshold. Spinal cord neurons in 4- to 7-day-old cultures exhibit spontaneous firing that is depressed by application of bicuculline to block $GABA_A$ receptors, suggesting that GABA release from developing axons can drive sodium APs (13). Similarly, a brief application of glycine onto the *in vitro* spinal cord isolated from fetal rats, at embryonic day 15.5 (i.e., 1 week before birth), evokes excitatory responses that are abolished by strychnine (14). Therefore, there is no doubt that GABA and glycine can play an excitatory role at an early stage of the development of spinal MNs and interneurons when E_{Cl} is above the AP threshold. The question of the excitatory and/or inhibitory nature of GABA/glycine is more difficult when E_{Cl} is negative to the threshold for APs but more positive than the resting membrane potential, which is the case in lumbar MNs during the first postnatal week in rats (1) and mice (15). The depolarization is sufficient to activate voltage-dependent calcium channels, remove the voltage-dependent magnesium block from NMDA channels, and induce a rise in intracellular calcium (16). It is generally accepted that, despite their depolarizing action, GABA/glycine can be inhibitory in immature spinal MNs because of the shunting action of the increased Cl^- conductance (4, 17–19). Evidence in support of this idea derives from experiments showing that depolarizing current pulses that produce APs in saline solution fail to evoke APs in the presence of GABA or glycine in the bath [spinal (18) and hypoglossal (19) MNs]. However, little is known about how depolarizing IPSPs (dIPSPs) interact with other synaptic inputs. The only report examining this issue in the spinal cord revealed that IPSPs evoked in MNs consistently inhibit excitatory PSPs (EPSPs) elicited at the top of the dIPSP (19). However, GABA was recently reported to have excitatory actions in the cortex (20) and hypothalamus (21). Beyond the developmental considerations, there is a need to understand these mechanisms because inhibitory amino acids depolarize neurons in some pathological conditions [i.e., neuronal damage, peripheral nerve-induced chronic pain, human temporal lobe epilepsy (22–26)], and recent findings demonstrate a spatial segregation of GABA-evoked depolarizing and hyperpolarizing responses in different compartments of individual interneuronal processes (27). In this study, we investigated the integration of dIPSPs with excitatory inputs in the neonatal rodent spinal cord. We define some of the conditions (e.g., timing, location, and E_{Cl}) under which GABA/glycinergic inputs can facilitate AP generation when paired with subthreshold excitatory inputs. Preliminary results have been presented.¶

Results

Duration of Inhibition Depends on E_{IPSP} and Location of Inhibitory Synapses. We examined the effective strength of inhibitory synapses by testing the ability of IPSPs to block APs evoked by depolarizing current pulses (referred to here as "functional inhibition"). Before being elicited concurrently, the ventral funiculus (VF) stimulation and the current pulses were first presented independently to measure the reversal potential of IPSPs (E_{IPSP}) and to adjust the intracellular current strength slightly above threshold (T) for AP generation ($<1.1 \times T$). In the MN shown in Fig. 1*A1*, the IPSP

Author contributions: C.J.-X. and L.V. designed research; C.J.-X., G.Z.M., and L.V. performed research; D.C. contributed new reagents/analytic tools; C.J.-X., G.Z.M., and L.V. analyzed data; and C.J.-X., G.Z.M., M.J.O., D.C., and L.V. wrote the paper.

The authors declare no conflict of interest.

Abbreviations: AP, action potential; PSP, postsynaptic potential; EPSP, excitatory PSP; IPSP, inhibitory PSP; dIPSP, depolarizing IPSP; MN, motoneuron; VF, ventral funiculus; *T*, threshold.

§To whom correspondence should be addressed. E-mail: vinay@dpm.cnrs-mrs.fr.

¶Jean-Xavier, C., Cattaert, D., Vinay, L. (2005) *Soc. Neurosci.*, Abstract 516.13.

This article contains supporting information online at www.pnas.org/cgi/content/full/0704832104/DC1.

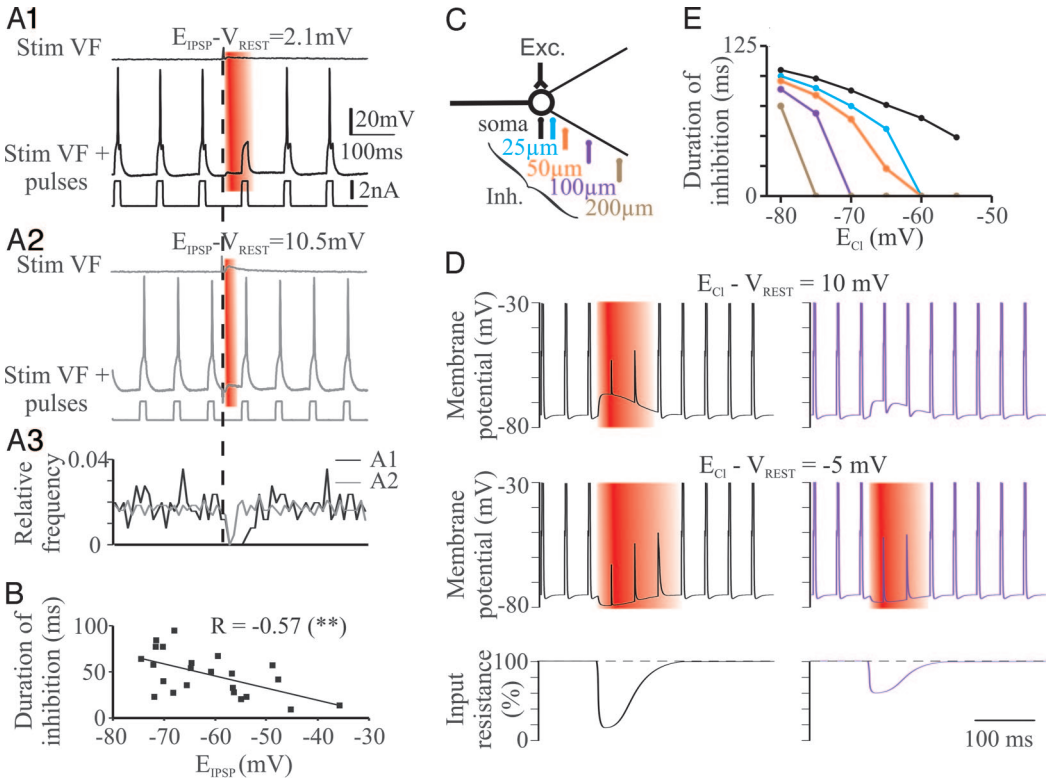

Fig. 1. E_{IPSP} and location of synapses affect the inhibitory action of IPSPs. (*A1* and *A2*) Responses evoked in L4 MNs by VF stimulation (vertical dotted line) in the absence (*Top*) or presence (*Middle*) of suprathreshold current pulses (*Bottom*). V_{REST} in both cases, −67 mV. Red, time window during which VF stimulation prevented the cells from firing. (*A3*) Frequency distributions of APs elicited by current pulses (black and gray traces, MNs shown in *A1* and *A2*, respectively). Same time scale as in *A1* and *A2*. (*B*) Duration of inhibition and E_{IPSP} are negatively correlated ($r = -0.57$; $n = 23$ MNs; $P < 0.01$, Pearson). (*C*) Compartment model used in simulations. Excitatory inputs were set on the soma, whereas inhibitory inputs were moved along the dendrites. (*D*) Depolarizing (*Top*) and hyperpolarizing (*Middle*) IPSPs generated on the soma (*Left*) and at 100 μm from the soma (*Right*). APs are truncated. V_{REST}, −75 mV. (*Bottom*) Changes in input resistance measured at the soma level. (*E*) Duration of functional inhibition (*D*, red) generated at the soma level by inhibitory synapses at different locations along dendrites, plotted against E_{Cl}.

elicited by VF stimulation was slightly depolarizing at resting membrane potential ($V_{REST} = -67$ mV; $E_{IPSP} = -64.8$ mV). The IPSP suppressed APs in a 55-ms time window after the onset. The MN shown in Fig. 1*A2* had a more depolarized E_{IPSP} (−56 mV). The ability of the IPSP to inhibit APs was reduced (28 ms) compared with the MN in Fig. 1*A1* (Fig. 1*A3*). Fig. 1*B* represents the duration of the functional inhibition for all of the MNs recorded as a function of E_{IPSP}. The duration decreased significantly as E_{IPSP} shifted toward more depolarized values. These results suggest that dIPSPs are less able to suppress suprathreshold excitatory events than hyperpolarizing IPSPs, suggesting that the depolarization counteracts and can overcome the shunting effect.

To better understand how E_{IPSP} and the location of inhibitory synapses affect the inhibitory action of IPSPs, we modeled the IPSP–EPSP interaction by means of the compartment model program "Neuron." V_{REST} was set to −75 mV, a realistic value for neonatal MNs (1). Consistent with our experimental observations, these simulations revealed that somatic IPSPs prevented AP initiation when paired with suprathreshold EPSPs ($1.07 \times T$) generated on the soma, whatever the value of E_{Cl} from −80 to −55 mV (Fig. 1*D*, black traces; Fig. 1*E*, black line and dots). This inhibitory effect reflects the conductance change accompanying the somatic IPSP (g_{inh}max = 120 nS). The kinetics of the chloride conductance associated with the inhibitory synapse was an α-function with a time constant of 15 ms (see *Materials and Methods*). The time courses of the conductance change and the resulting IPSP are indicated in supporting information (SI) Fig. 5. The duration of this inhibition decreased significantly as E_{Cl} was set to more depolarized values (correlation, $P < 0.0001$). We next investigated the influence of IPSP location on the suppression of AP generated by somatic EPSPs. The time window of functional inhibition became shorter as the inhibitory synapses were moved to 25 μm away from the soma (Fig. 1*E*, blue line and dots; slopes of regression lines from −80 to −65 mV were significantly different; $P < 0.05$; data not shown). A further shortening was observed as the inhibitory synapses were moved toward apical dendrites (Fig. 1*D Bottom*, violet trace; Fig. 1*E*, orange, violet, and brown lines for IPSPs generated at 50, 100, and 200 μm from the soma, respectively). Moving IPSP location along the dendrites reduced the range of E_{Cl} for which IPSPs prevented AP initiation on the top of suprathreshold EPSPs ($1.07 \times T$) generated on the soma. For instance, dIPSPs generated at 100–200 μm from the soma did not inhibit EPSP-induced firing (Fig. 1*E*, violet and brown lines). The effect of slight changes in E_{Cl} on the duration of functional inhibition was more important for distal than somatic inhibitory inputs as shown by the steepest curves (Fig. 1*E*). These results show that the ability of IPSPs to be inhibitory depends not only on the conductance changes, but also on the amplitude of the hyperpolarization or depolarization and the location of inhibitory synapses.

Shunting Action Is Local, Whereas Depolarization Spreads Electrotonically. The duration of the time window over which IPSPs blocked the evoked APs (functional inhibition) was correlated with the duration of the depolarization ($r = 0.35$, $n = 37$ MNs; $P < 0.05$, Pearson; data not shown). However, the duration of functional inhibition was significantly shorter than that of IPSP (47.3 ± 3.7 ms and 136 ± 12.4 ms, respectively; $n = 37$; $P < 0.0001$; paired t test; data not shown). To better understand the reason for the mismatch

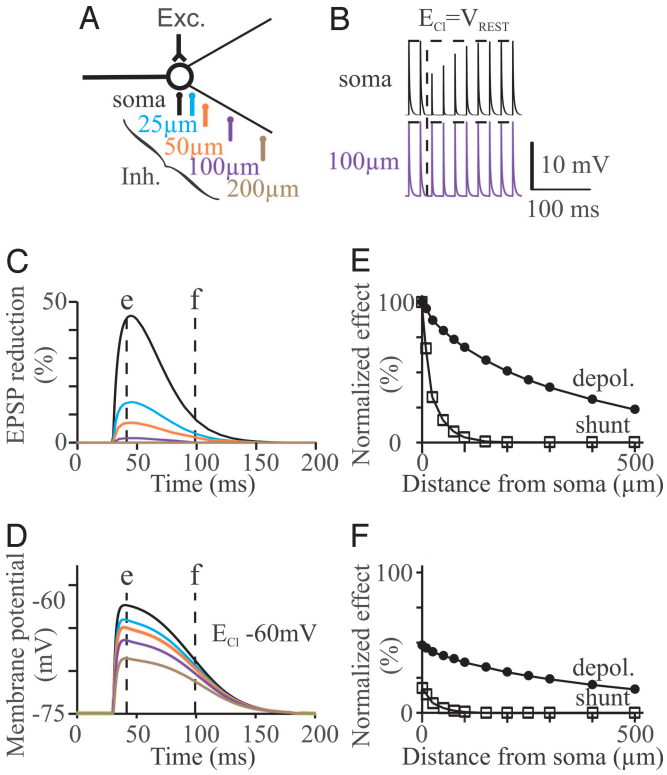

Fig. 2. Electrotonic spread of dIPSPs. (*A*) Model. (*B*) Effect on trains of somatic subthreshold EPSPs of IPSPs generated on the soma and at 100 μm on dendrites. (*C*) Time course of the IPSP-induced reduction of the somatic EPSP for different locations of inhibitory synapses (same colors as in *A*). E_{Cl} was set at V_{REST} to prevent any change in membrane potential. (*D*) Time course of membrane potential changes at the soma level induced by dIPSPs generated at different loci. (*E* and *F*) Effects of IPSPs on both the somatic membrane potential and reduction of somatic EPSPs ("shunt"), plotted against the location of inhibitory synapses. Both parameters are normalized relative to the maximal effect observed when inhibitory synapses are set to the soma (black trace at time $t = e$ in *C* and *D*). *E* and *F* correspond to the values obtained at times $t = e$ and $t = f$, respectively, in *C* and *D*.

between these two durations, we examined the timing and propagation of both the conductance change and depolarization in the model. Subthreshold EPSPs were evoked in the soma (Fig. 2*B*). IPSPs were generated at different somatic and dendritic locations (Fig. 2*A*) with E_{Cl} set to -75 mV ($E_{Cl} = V_{REST}$), meaning that the conductance increase was not associated with any effect on the membrane potential of the cell model. The amplitude of EPSP was measured. Inhibitory synapses generated on the soma caused a 45% reduction of EPSP amplitude (Fig. 2*B*; onset of inhibition indicated by vertical dotted line; Fig. 2*C*, black line). The inhibition markedly decreased as the inhibitory input was slightly moved away from the soma. The EPSP was reduced by only 14% and 7% with inhibitory synapses at 25 and 50 μm from the soma, respectively (Fig. 2*C*, blue and orange lines). Synapses at 100 μm and farther had little effect (<2% reduction of the EPSP; Fig. 2 *B Lower* and *C*, violet and brown lines).

We next examined the spread of the depolarization when E_{Cl} was above V_{REST}. E_{Cl} was set to -60 mV, and inhibitory inputs were evoked at different somatic and dendritic locations (Fig. 2*D*). The effects of IPSPs on both EPSPs amplitude ("shunting effect") and the membrane potential recorded from the soma were normalized relative to the maximal effect observed when inhibitory synapses were set to the soma (Fig. 2 *E* and *F* plotting the values obtained at times $t = e$ and $t = f$, respectively, in Fig. 2 *C* and *D*). With inhibitory synapses on the soma, 70 ms after the IPSP onset (at time $t = f$ in Fig. 2 *C* and *D*), the membrane potential was still depolarized at 48% of the maximal amplitude, whereas the shunting effect had markedly decreased to 17% (Fig. 2*F*), thereby confirming that the time course of the conductance change is faster than that of the resulting IPSP (SI Fig. 5) because of the relationship between the membrane potential V and the ionic current i that permeates through the opened chloride channel ($dV/dt = i/c_m$, with c_m the membrane capacitance).

The depolarization induced in the soma slightly decreased as the inhibitory synapses were moved from 0 to 500 μm from the soma, whereas the conductance increase dropped within 50 μm (Fig. 2 *C–F*). Therefore, the major conclusion is that the depolarization spreads electrotonically as inhibitory synapses are moved away from the soma, whereas the shunting is local.

Excitatory Actions of dIPSPs. Depolarizing IPSPs never reached AP threshold in any of the recorded cells. We investigated the interaction of dIPSPs with subthreshold excitatory events occurring at different times during depolarization. In the *in vitro* spinal cord, we combined dIPSPs with subthreshold depolarizing current pulses injected into MNs. These pulses induced a much smaller depolarizing potential when applied at around the peak of the IPSP presumably because of the shunting effect (Fig. 3*A*, red). By contrast, when occurring on the decay phase of the synaptic response, the pulse triggered an AP. The facilitation (Fig. 3*A*, green) started at a time when there was no more blockade of current-evoked APs, but the neuron was still depolarized (onset of facilitation, 72.5 ± 14.9 ms, $n = 11$; end of functional inhibition, 51.4 ± 8 ms, $n = 8$; correlation between these two parameters, $r = 0.80$, $n = 8$; $P < 0.05$, Spearman). The onset of the facilitation was correlated with both E_{IPSP} ($r = -0.62$, $n = 11$; $P < 0.05$, Spearman) and the duration of IPSPs ($r = 0.8$, $n = 11$; $P < 0.01$, Spearman). Note that in three cells the facilitation started quite early, at around the peak of the IPSP, which is after the peak of the conductance change (SI Fig. 5); these neurons had a depolarized E_{IPSP} (-43.7 mV in average). To further determine whether the facilitation was because of depolarization or a possible decreased conductance, we calculated the time constant of the MN membrane. A nonsignificant trend toward a decrease was observed in the time window during which there was the facilitation (-17%; $P > 0.05$; $n = 6$). These results suggest that the IPSP-mediated facilitation of subthreshold excitatory currents was critically dependent on the amplitude and duration of the dIPSP and likely results from the fact that the membrane potential remains above AP threshold, whereas the conductance change has decayed back to control levels.

We modeled the interaction between dIPSPs and subthreshold ($\approx 0.92 \times T$) EPSPs. As was observed physiologically with depolarizing current pulses, the IPSP promoted AP firing if the paired subthreshold EPSP was timed to occur on the decay phase of the IPSP (Fig. 3*B*). Changing the delay between inhibitory and excitatory inputs enabled us to measure the timing and duration of the facilitation. The window of facilitation became wider as E_{Cl} was set to more depolarized values (Fig. 3*D*) and started earlier as inhibitory synapses were displaced distally along dendrites (Fig. 3*D*). As a result, inhibitory inputs located at 100 μm from the soma had a facilitatory action on somatic excitatory inputs over the whole duration of the dIPSP (Fig. 3*D*). Note that this facilitation occurred with E_{Cl} set to relatively hyperpolarized values (-65 mV at 100 μm and -69 mV at 200 μm; i.e., only 6–10 mV above V_{REST}) and EPSPs with an amplitude set to $0.85 \times T$. By contrast, a facilitation induced by somatic inhibitory inputs required E_{Cl} to be set to values more positive than -53 mV (Fig. 3*C*, black). Facilitatory action on distant excitatory inputs was observed regardless of the location of the inhibitory and excitatory synapses. Somatic inhibitory inputs were indeed able to promote AP firing when paired with subthreshold EPSPs generated by synapses at 200 μm from the soma (SI Fig. 6).

We combined both the inhibitory and excitatory actions of IPSPs

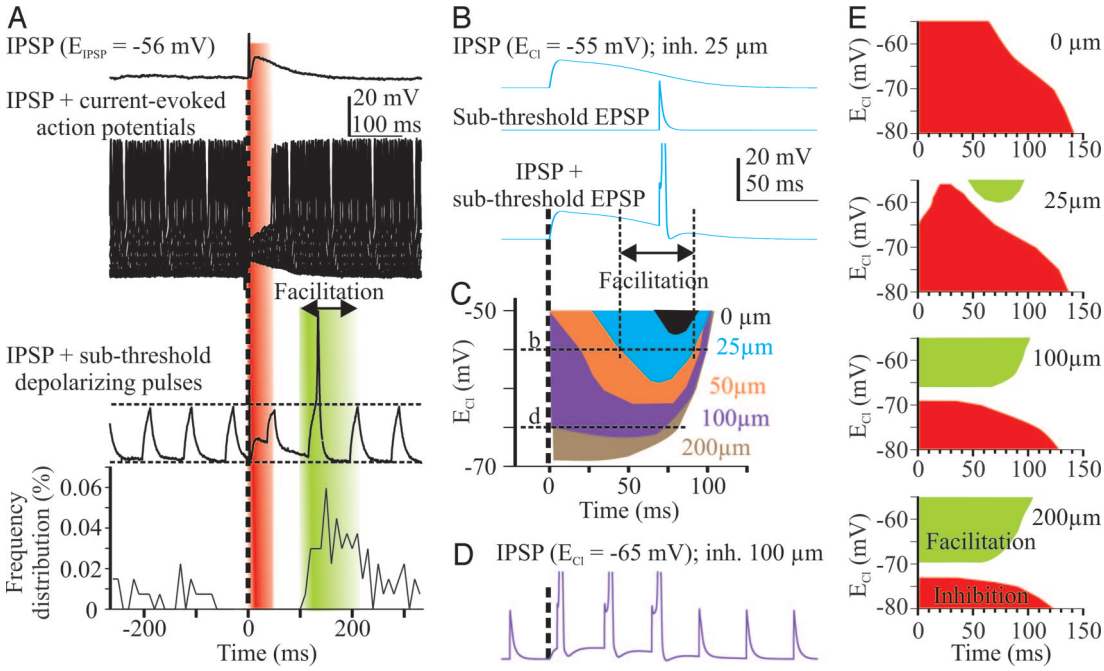

Fig. 3. Excitatory actions of dIPSPs. (*A*) VF stimulation-evoked response in an L4 MN in the absence (*Top*) or presence of current pulses (suprathreshold: *Middle*, 50 sweeps; subthreshold: *Bottom*, single sweep). V_{REST} = −68 mV. Histogram represents the frequency distribution of APs elicited by current pulses of the same magnitude, which were most often (98%) subthreshold when delivered before VF stimulation (t = 0). (*B*) Inhibition (at 25 μm from soma; E_{Cl} = −55 mV) and subthreshold excitation (at the soma) presented independently (*Top* and *Middle*) or concurrently (*Bottom*) in the compartment model. (*C*) Time windows of the dIPSP-evoked facilitation of cell firing at different values of E_{Cl}. Colors correspond to different loci for inhibitory synapses. (*D*) Subthreshold EPSPs trigger APs during the whole duration of the IPSP evoked at 100 μm from soma. Note the hyperpolarized value of E_{Cl} (−65 mV). (*E*) Global pictures of inhibitory (inhibition of suprathreshold EPSPs) and excitatory (facilitation of subthreshold EPSPs) effects depending on both E_{Cl} and the location of inhibitory inputs.

on the same graphs to get the global picture of the conditions (timing, location, and E_{Cl}), under which IPSPs can facilitate or inhibit AP generation, when paired with sub- or suprathreshold excitatory inputs, respectively (Fig. 3*E*). Inhibitory inputs on the soma had only inhibitory actions regardless of the value of E_{Cl} within the −55- to −80-mV range. Proximal inputs (e.g., 25 μm) had an inhibitory effect for E_{Cl} less than −60 mV. For more depolarized E_{Cl} values, the effect was strongly dependent on the timing, with inhibitory action occurring early in the IPSP and facilitation occurring later (Fig. 3 *B* and *E*). Interestingly, this temporal separation was not observed in the case of more distal inhibitory inputs (Fig. 3*E*; 100–200 μm) for which a slight depolarizing shift of E_{Cl} (3–5 mV) within a range of potentials close to V_{REST} (less than −65 mV) was able to switch the action of inhibitory synapses from inhibition to facilitation. The global picture of the excitatory and inhibitory effects was not markedly changed by modifying the time constant (Tau_{inh}) of IPSPs (SI Fig. 7). Note also that the spread of the conductance change does not depend on the space constant. By contrast, the spread of depolarization, and therefore the facilitatory action of dIPSPs, increases with space constant (simulations not shown; see *SI Text*). These results reveal the dual personality of distal inhibitory inputs; the expression of either the inhibitory or excitatory actions relies on the critical regulation of E_{Cl}.

Presence of GAD65/67 Immunoreactive Synaptic Boutons on Distal Dendrites of Neonatal MNs. To establish whether inhibitory inputs are observed on the distal part of dendrites in the neonatal spinal cord, eight MNs (five identified from the L5 ventral root and three from the L4 ventral root) were analyzed and quantified in terms of the immunoreactive sites for the GAD65/67 antibody and are presumed to be GABAergic boutons. The average somatic area through the largest plane of the soma was 401.1 μm^2 (n = 8). Putative GABAergic synaptic boutons were observed throughout the somatodendritic tree of the MNs (see Fig. 4). We analyzed 26 dendrites emerging from the soma (primary dendrites; 0–25 μm in length), 30 dendrites of 25–50 μm distance from the soma, 21 dendrites of 50–100 μm from the soma, 20 dendrites of 100–200 μm from the soma, and 4 dendrites of 200–250 μm from the soma.

The synaptic bouton size was measured randomly for all four dendritic lengths and around the soma. We measured 516 synaptic boutons that were immunoreactive for GAD65/67. There was no statistical difference in the size of GAD65/67-positive synaptic boutons between the soma and any of the dendritic lengths (around soma, 1.05 ± 0.05 μm, n = 55; 1.07 ± 0.03 μm in 0- to 25-μm dendrites, n = 84; 1.05 ± 0.03 μm in 25- to 50-μm dendrites, n = 87; 1.08 ± 0.02 μm in 50- to 100-μm dendrites, n = 138; and 1.02 ± 0.02 μm in 100- to 200-μm dendrites, n = 152).

GAD65/67 immunoreactive boutons were observed on the soma (Fig. 4*B*) as well as on all dendrites of the MNs (Fig. 4 *C* and *D*). GAD65/67-positive boutons were observed in all dendrites analyzed except one. No difference in the synaptic coverage was observed between different projection dendrites. There were, on average, 8 boutons around the soma of the MN and ≈3 boutons per 25 μm of dendritic length for the first 50 μm of the dendrite (Fig. 4*E*). The number of boutons slightly increased to 3.8 per 25 μm for more distal dendrites (50–100 μm); there was a nonsignificant trend toward a reduction to ≈1.5 per 25 μm for the most distal dendrites (200–250 μm; $P > 0.05$; one-way ANOVA). In some instances, immunoreactive boutons were observed to make contact with spines emanating from distal dendrites (Fig. *4D3*, white double arrowhead). Altogether these results suggest the existence of distal inhibitory synapses on MNs in the neonatal rodent spinal cord, in agreement with data on adult cats (28, 29).

Discussion

We report here that dIPSPs can either inhibit/shunt or facilitate other depolarizing potentials depending on three factors: (*i*) the

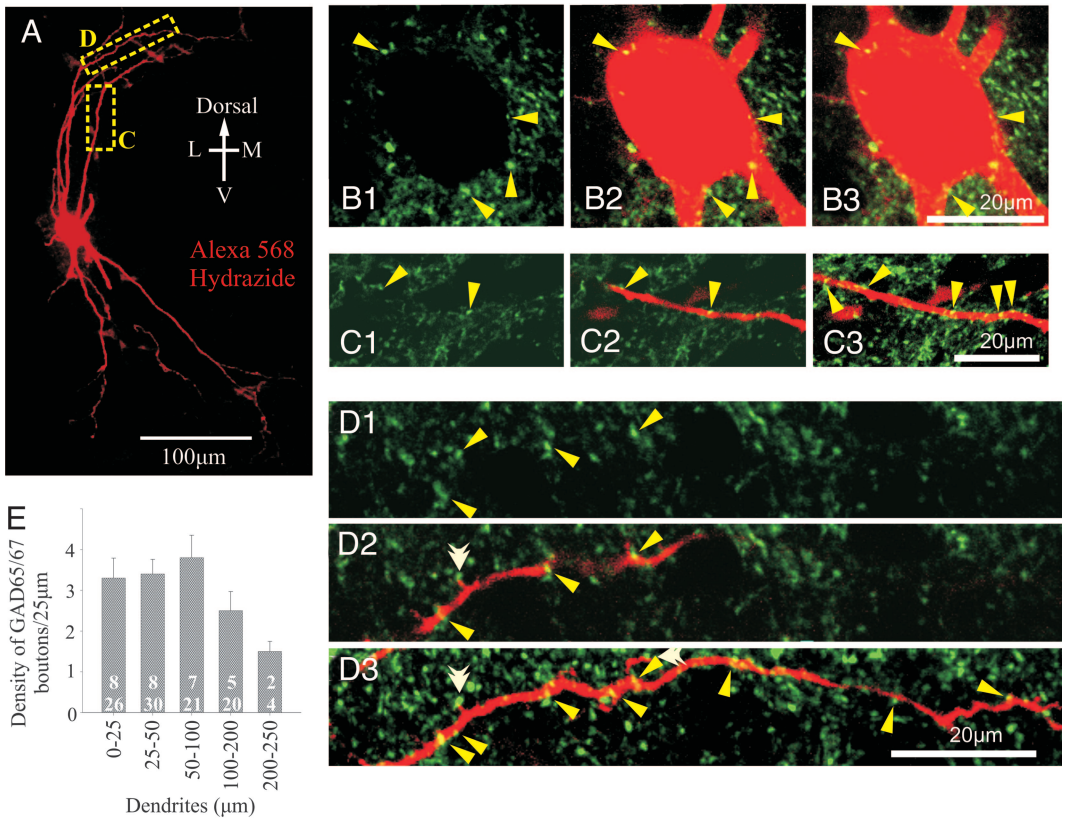

Fig. 4. Presence of GAD65/67 immunoreactive synaptic boutons on the soma and dendrites of neonatal MNs. (*A*) A 2D reconstruction from confocal images acquired in the *z* axis of a P3 MN filled intracellularly with Alexa 568 Hydrazide. (*B1*, *C1*, and *D1*) GAD65/67 immunoreactivity scanned at a single optical plane (thickness, 0.39 μm). (*B2*, *C2*, and *D2*) Single optical planes (as in *B1*, *C1*, and *D1*) showing superimposed GAD65/67 immunoreactivity and the various aspects of MN morphology (red). (*B3*, *C3*, and *D3*) Projection images from several optical planes demonstrating multiple sites of contact (arrows). Total thickness: *B3*, 2.3 μm; *C3*, 2.7 μm; *D3*, 3.5 μm. The white double arrowheads in *D3* show putative contact points on dendritic spines. (*B1*) GAD65/67. (*B 2* and *3*) GAD65/67 plus Alexa 568 Hydrazide. (*C*) Dendritic extent: 50–100 μm. (*D*) Dendritic extent: 100–200 μm. (*E*) Density measurements of GAD65/67-positive boutons on the different loci of MNs per 25 μm. Numbers of MNs (*Upper*) and dendrites (*Lower*) analyzed are indicated .

E_{Cl} relative to V_{REST}, (*ii*) the relative timing between the IPSP and the other excitatory inputs, and (*iii*) the location of inhibitory synapses on the somatodendritic tree. When E_{Cl} is between V_{REST} and the AP threshold, the effect on excitability depends on the relative weight of the inhibitory action of the conductance change and the excitatory action of the depolarization (20, 30). These actions have different time courses, such that the excitation dominates in the late part of the IPSP. More important, the conductance change is a local effect, whereas the depolarization spreads electrotonically. As a consequence, inhibitory synapses inhibit local excitations and exert a facilitatory action on distant excitatory inputs. Facilitation may be observed with values of E_{Cl} quite close to V_{REST}.

Periodic spontaneous activity is generated by the immature spinal cord (14, 31–35) and other networks of the CNS (36). It is widely believed to participate in the functional and structural maturation of these developing networks (37, 38). There are marked changes in the neurotransmitters responsible for the genesis and modulation of this spontaneous activity. At the earliest stages, cholinergic and glycinergic transmission are primarily responsible for the activity (35, 39). At this age, application of glycine to the spinal cord, *in vitro*, triggers bursts discharges in ventral roots, suggesting that E_{Cl} is more positive than the AP threshold. At the latest stages, the activity relies mainly on glutamatergic transmission. During the middle stage, the spontaneous activity involves non-NMDA glutamatergic, nicotinic acetylcholine, glycine, and $GABA_A$ receptors. All of these transmitter/receptor systems provide a component of excitation necessary to achieve rhythmicity (35).

The circuit generating these activities exhibits considerable plasticity, such that, for instance, after blockade of glutamatergic synaptic transmission, spontaneous bursting in the chick spinal cord recovers and is, at that time, driven by glycinergic and GABAergic connections (40, 41). The present results can fully account for the synergistic actions of different transmitter systems in spontaneous bursting, when E_{Cl} in MNs [−55/−65 mV in the perinatal rat (18)] is below the threshold potential for the inward sodium currents (42). At that stage, inhibitory amino acids may indeed promote network bursting by providing a subthreshold depolarization, on the top of which cholinergic and glutamatergic EPSPs are able to reach the firing threshold. A key action of GABA and glycine on distal dendrites would be to increase the general excitability of the soma and proximal dendrites; this action may be tonic and/or phasic. The GABA/glycinergic input may exert a temporally nonpatterned, facilitatory action in the generation of network events, as proposed recently in the hippocampus (43). In agreement with such a possibility in the spinal cord, a tonic $GABA_A$ current has been demonstrated in chicken embryo MNs (44); this current can depolarize neurons by ≈8 mV. Alternatively, a phasic GABA/glycinergic input on distal dendrites may convert a tonic subthreshold excitatory input into a phasic response. MN firing activates Renshaw cells, which provide a recurrent GABA/glycinergic facilitatory feedback drive on MNs. An important point in the two previously proposed mechanisms is the characteristic slow decay of

the dIPSPs in immature MNs (45), which offers a large time window for the facilitation of excitatory events.

The KCC2 cotransporter is sensitive to subtle changes in either $[Cl^-]_i$ or $[K^+]_o$ so that it can operate in reverse mode in the presence of high $[K^+]_o$ and contribute to Cl^- accumulation (46). The neuronal activity in the spinal cord in response to repetitive electrical stimulation of afferent fibers increases $[K^+]_o$ by as much as 6.5 mM in neonates and by ≈2–3.5 mM in adults (47). The Cl^- accumulation resulting from such elevated $[K^+]_o$ may cause a 9- to 15-mV positive shift of E_{IPSP} (24, 48). $[Cl^-]_i$ undergoes significant changes during spontaneous activity, leading to rhythmic variations of E_{Cl} of ≈15 mV (44, 49). Similarly, a down-regulation of KCC2 in pathological conditions can cause a ≈20-mV positive shift of E_{Cl} (26). In addition, there is increasing evidence that different subcellular compartments of individual neurons can express two distinct types of cation-chloride cotransporters so that a single neurotransmitter depolarizes or hyperpolarizes the different compartments (27, 50). Consistent with this observation, changes in $[Cl^-]_i$ during spontaneous motor episodes are larger in MN dendrites than at the soma level in the chicken embryo (49). The present results show that all these variations may have profound consequences on the excitability of the soma and dendrites and the integration of excitatory inputs. The present study indeed revealed that a 10-mV positive shift of E_{IPSP} may cause a marked (≈25 ms) shortening of the functional inhibition produced by inhibitory inputs on the soma or close to it (Fig. 1 *B* and *E*). In addition, simulations made for distal inhibitory inputs showed that there is a narrow range of E_{Cl} (from approximately −73 to −66 mV), around V_{REST}, within which the functional action of these inhibitory inputs can switch from inhibition to facilitation (Fig. 3*E*).

To conclude, these results raise the possibility that dIPSPs in the spinal cord are not relics of the past (i.e., the early stages of fetal development when GABA and glycine were purely excitatory), but are instead a sophisticated mechanism for regulating the integrative capability of the neuron and shaping the temporal properties of network activity. The presence of GABA/glycine in presynaptic terminals is therefore a necessary, but not sufficient, requirement for postsynaptic inhibition to occur. The inhibitory effect depends on the location and timing of inhibitory inputs relative to excitatory inputs and E_{Cl}, which is critically dependent on the recent experience of the neuron (48). The functional compartmentalization of dendrites, based on the differential expression of cation-chloride cotransporters (27), raises the possibility that GABA/glycine could facilitate glutamate-evoked excitation along a portion of a process and inhibit it elsewhere along the same process. This possibility warrants further studies to investigate how these interactions between GABA/glycine and glutamate inputs at different subcellular levels contribute to neuronal computations in physiological and pathological conditions.

Materials and Methods

Further experimental details and data are given in *SI Text* and SI Figs. 5–7.

Electrophysiological Experiments. Lumbar MNs were recorded intracellularly by using sharp microelectrodes filled with 2 M K-acetate. The VF of the spinal cord was stimulated by means of suction electrodes to evoke glycine/GABAergic IPSPs that were isolated pharmacologically (1). The AP T was determined by injecting positive current pulses (14–20 ms, 0.8–2.8 nA). Suprathreshold (1.04–1.5 × *T*) and subthreshold (0.8–0.92 × *T*) current pulses were paired with an IPSP to determine the "functional inhibition" (defined as the time window during which the APs were blocked) and the time window of facilitation, respectively. Note that either repetitive (≈10 Hz) or single (with different delays) pulses were used; no difference was observed between the two protocols.

Simulations. The interactions between IPSPs and EPSPs were simulated by using the program NEURON 5.6. The compartment model was made of a cell body (diameter 20 μm), two dendrites (length 500 μm; diameter 2 μm), and an axon (length 500 μm; diameter 1 μm). Axon and dendrites were made of 21 segments each. The properties of each compartment could be defined independently. Dendritic compartments received synaptic inputs (EPSP/IPSP), the location of which could be set at any position along one of the dendrites. The density of the synaptic inputs could be set independently for EPSP and IPSPs.

Immunohistochemistry. MNs were recorded with patch electrodes filled with Alexa 568 Hydrazide. After fixation, spinal cords were cut transversally into 70-μm sections. Immunohistochemistry was performed by using a GAD65/67 antibody and a secondary antibody conjugated to FITC. Sections were observed on a confocal microscope.

This work was supported by the French Ministry for Research, Integrative and Computational Neuroscience Program (C.J.-X.), the French Institute for Spinal Cord Research, the NRJ Foundation, the Christopher and Dana Reeve Foundation Grant VB1–0502-2 (to L.V.), and in part by the Intramural Research Program of the National Institutes of Health/National Institute of Neurological Disorders and Stroke (G.Z.M. and M.J.O.).

1. Jean-Xavier C, Pflieger J-F, Liabeuf S, Vinay L (2006) *J Neurophysiol* 96:2274–2281.
2. Vinay L, Brocard F, Pflieger JF, Simeoni-Alias J, Clarac F (2000) *Brain Res Bull* 53:635–647.
3. Obata K, Oide M, Tanaka H (1978) *Brain Res* 144:179–184.
4. Wu W-L, Ziskind-Conhaim L, Sweet MA (1992) *J Neurosci* 12:3935–3945.
5. Ben-Ari Y, Cherubini E, Corradetti R, Gaiarsa JL (1989) *J Physiol (Lond)* 416:303–325.
6. Reichling DB, Kyrozis A, Wang J, MacDermott AB (1994) *J Physiol* 476:411–421.
7. Chen G, Trombley PQ, van den Pol AN (1996) *J Physiol* (*Lond*) 494:451–464.
8. Owens DF, Boyce LH, Davis MB, Kriegstein AR (1996) *J Neurosci* 16:6414–6423.
9. Luhmann HJ, Prince DA (1991) *J Neurophysiol* 65:247–263.
10. Ehrlich I, Lohrke S, Friauf E (1999) *J Physiol* 520:121–137.
11. Kakazu Y, Akaike N, Komiyama S, Nabekura J (1999) *J Neurosci* 19:2843–2851.
12. Lee MT, Koebbe MJ, O'Donovan MJ (1988) *J Neurosci* 8:2530–2543.
13. Gao XB, van den Pol AN (2001) *J Neurophysiol* 85:425–434.
14. Nishimaru H, Iizuka M, Ozaki S, Kudo N (1996) *J Physiol* 497:131–143.
15. Stein V, Hermans-Borgmeyer I, Jentsch TJ, Hubner CA (2004) *J Comp Neurol* 468:57–64.
16. Kulik A, Nishimaru H, Ballanyi K (2000) *J Neurosci* 20:7905–7913.
17. Baccei ML, Fitzgerald M (2004) *J Neurosci* 24:4749–4757.
18. Gao B-X, Ziskind-Conhaim L (1995) *J Neurophysiol* 74:113–121.
19. Marchetti C, Pagnotta S, Donato R, Nistri A (2002) *Eur J Neurosci* 15:975–983.
20. Gulledge AT, Stuart GJ (2003) *Neuron* 37:299–309.
21. Gao XB, Chen G, van den Pol AN (1998) *J Neurophysiol* 79:716–726.
22. Cohen I, Navarro V, Clemenceau S, Baulac M, Miles R (2002) *Science* 298:1418–1421.
23. Toyoda H, Ohno K, Yamada J, Ikeda M, Okabe A, Sato K, Hashimoto K, Fukuda A (2003) *J Neurophysiol* 89:1353–1362.
24. Payne JA, Rivera C, Voipio J, Kaila K (2003) *Trends Neurosci* 26:199–206.
25. Nabekura J, Ueno T, Okabe A, Furuta A, Iwaki T, Shimizu-Okabe C, Fukuda A, Akaike N (2002) *J Neurosci* 22:4412–4417.
26. Coull JA, Boudreau D, Bachand K, Prescott SA, Nault F, Sik A, De Koninck P, De Koninck Y (2003) *Nature* 424:938–942.
27. Gavrikov KE, Nilson JE, Dmitriev AV, Zucker CL, Mangel SC (2006) *Proc Natl Acad Sci USA* 103:18793–18798.
28. Alvarez FJ, Dewey DE, Harrington DA, Fyffe RE (1997) *J Comp Neurol* 379:150–170.
29. Brannstrom T (1993) *J Comp Neurol* 330:439–454.
30. Stein V, Nicoll RA (2003) *Neuron* 37:375–378.
31. Vinay L, Brocard F, Pflieger J, Simeoni-Alias J, Clarac F (2000) *Brain Res Bull* 53:635–647.
32. Vinay L, Brocard F, Clarac F, Norreel JC, Pearlstein E, Pflieger JF (2002) *Brain Res Rev* 40:118–129.
33. O'Donovan MJ (1999) *Curr Opin Neurobiol* 9:94–104.
34. Nakayama K, Nishimaru H, Iizuka M, Ozaki S, Kudo N (1999) *J Neurophysiol* 81:2592–2595.
35. Ren J, Greer JJ (2003) *J Neurophysiol* 89:1187–1195.
36. Ben-Ari Y (2001) *Trends Neurosci* 24:353–360.
37. Spitzer NC, Root CM, Borodinsky LN (2004) *Trends Neurosci* 27:415–421.
38. Feller MB (1999) *Neuron* 22:653–656.
39. Hanson MG, Landmesser LT (2003) *J Neurosci* 23:587–600.
40. Chub N, O'Donovan MJ (1998) *J Neurosci* 18:294–306.
41. Milner LD, Landmesser LT (1999) *J Neurosci* 19:3007–3022.
42. Gao BX, Ziskind-Conhaim L (1998) *J Neurophysiol* 80:3047–3061.
43. Sipila ST, Huttu K, Soltesz I, Voipio J, Kaila K (2005) *J Neurosci* 25:5280–5289.
44. Chub N, O'Donovan MJ (2001) *J Neurophysiol* 85:2166–2176.
45. Singer JH, Talley EM, Bayliss DA, Berger AJ (1998) *J Neurophysiol* 80:2608–2620.
46. Payne JA (1997) *Am J Physiol* 273:C1516–C1525.
47. Sykova E, Jendelova P, Svoboda J, Chvatal A (1992) *Can J Physiol Pharmacol* 70(Suppl):S301–S309.
48. Lamsa K, Taira T (2003) *J Neurophysiol* 90:1983–1995.
49. Chub N, Mentis GZ, O'Donovan MJ (2006) *J Neurophysiol* 95:323–330.
50. Marty S, Wehrle R, Alvarez-Leefmans FJ, Gasnier B, Sotelo C (2002) *Eur J Neurosci* 15:233–245.